ORIGINAL ARTICLE

α-Titanium phosphate intercalated with propylamine: An alternative pathway for efficient europium(III) uptake into layered tetravalent metal phosphates

CrossMark

Jorge García-Glez [a], Camino Trobajo [a], Sergei A. Khainakov [b], Zakariae Amghouz [b,*]

[a] *Department of Organic and Inorganic Chemistry, University of Oviedo-CINN, 33006 Oviedo, Spain*
[b] *Scientific and Technical Services, University of Oviedo-CINN, 33006 Oviedo, Spain*

Abstract   α-Ti(HPO$_4$)$_2$·H$_2$O (α-TiP) and its propylamine intercalation product, Ti(HPO$_4$)$_2$·2C$_3$H$_7$NH$_2$·H$_2$O (α-TiPPr), have been synthesized and characterized. Later, their sorption capacity for europium(III) was investigated, and this purpose was accomplished by treating α-TiP and α-TiPPr with europium(III) nitrate solutions at different concentrations until the equilibrium is reached. All samples were characterized, among others, by powder X-ray diffraction (PXRD), scanning and transmission electron microscopies (SEM, TEM, STEM-EDX, SAED), thermogravimetric analysis (TGA), and photoluminescence (PL) measurements. The results show that the Eu^{3+} uptake is limited to surface when α-TiP is used as sorbent. Nevertheless, the Eu-retention is considerably enhanced with α-TiPPr as a consequence of an ion-exchange process into the interlayer space of the layered titanium phosphate (involving propylammonium cations, C$_3$H$_7$NH$_3^+$, and hexahydrate europium(III) species, [Eu(H$_2$O)$_6$]$^{3+}$), and the crystal structure of a hypothetical final product, α-[Eu(H$_2$O)$_6$]$_{2/3}$Ti(PO$_4$)$_2$·[(H$_2$O)$_6$]$_{1/3}$, has been proposed by using DFT calculations.

1. Introduction

Recently, Ortíz-Oliveros et al. (2014) have published the synthesis, physical-chemical characterization and preliminary evaluation of α-Ti(HPO$_4$)$_2$·H$_2$O (α-TiP) sorption of Eu^{3+}, which is often considered as a chemical analogue for trivalent heavy metals, lanthanides and also actinides (such as Np, Am, Cm and Pu, radionuclides found in high-level radioactive waste produced during the nuclear fuel cycle). The authors concluded that the retention process for Eu^{3+} can take place on the surface and in the cavities of the solid in two stages: (a) diffusion into the cavities of the material and (b) chemisorption. In this work, we will show that the uptake process is, in fact, limited to the surface of

the α-titanium phosphate (the interlayer space is inaccessible to the europium species when the α-TiP hydrogen form is used as sorbent), while the diffusion into internal cavities is only possible when basal spacing is previously expanded (e.g., intercalated by propylamine).

Ortíz-Oliveros et al. (2014) addressed, among other things, the evaluation of Eu^{3+} sorption capacity by crystalline α-TiP, based on the fact that the titanium and zirconium phosphates, and other isomorphic tetravalent metal phosphates α-M(HPO$_4$)$_2$·H$_2$O (M = Zr, Ti, Sn, etc.) have been successfully used in the recovery of uranium, plutonium and fission products (Zhuravlev et al., 2002; Mrad et al., 2011). However, Zhuravlev et al. (2002) relied on the use of amorphous samples of titanium and zirconium phosphates (modified with Al^{3+} or Fe^{3+} ions during the gelation process), whereas Mrad et al. (2011) carried out their work using semi-crystalline Zr(HPO$_4$)$_2$·H$_2$O (where an adsorption occurs on the surface, and an ion-exchange mechanism is not fully confirmed).

Metal salts of phosphoric acid have been known for over a century. Because of their extraordinary properties, a great variety of potential and realized uses have been invoked. Among the many uses in addition to both ion-exchange and intercalation-chemistry are catalysis, polymer composites, proton conduction, drug delivery and many others, such as energy storage, sensors and biosensors, flame retardants, and antibiomaterials (Clearfield and Díaz, 2015). Titanium phosphate can be prepared either as gel or in intermediate stages of crystallinity, but also in several crystalline forms including γ-Ti(PO$_4$)(H$_2$PO$_4$)·2H$_2$O (γ-TiP) and α-TiP (Salvadó et al., 1996; García-Granda et al., 2010), being known that the main factors affecting the ion-exchange behavior of tetravalent metal phosphates are their structures and the degree of crystallinity (Llavona et al., 1989). α- and γ-TiP are layered compounds with flexible two-dimensional structures that, although they have ion-exchange properties, display low affinity toward both transition and inner transition metal ions (Álvarez et al., 1987; Trobajo et al., 1991). The synthesis of ion-exchange phases with polyvalent cations is possible by means of an indirect route. In the first stage, the reaction between the inorganic solid acid (α- or γ-TiP) and the vapor of an organic base (e.g., n-alkylamine), produced an essentially non-porous intercalation compound (Menéndez et al., 1993; Espina et al., 1998a, 1998b), usually with strong preferential orientation effects and thermal disorder of the alkyl chains (Mafra et al., 2005, 2008). In a second step, the intercalation compound reacts with an aqueous solution of the desired metal salt, and the substitution of intercalated organic cation by the inorganic metal cation takes place (Trobajo et al., 1991; Alfonso et al., 2005).

In this paper, α-TiP intercalated with propylamine (α-TiPPr) has been selected to investigate its sorption of Eu(III) by means of PXRD, SEM, TEM, TGA and PL, Moreover, the structural modeling of a hypothetical full ion-exchange phase, [Eu(H$_2$O)$_6$]$_{2/3}$Ti(PO$_4$)$_2$·[(H$_2$O)$_6$]$_{1/3}$, has been also proposed on the basis of DFT calculations.

2. Materials and methods

2.1. Synthesis of sorbents

All chemicals used were of reagent grade. MilliQ water was used throughout the experiments. α-TiP was obtained by the method described by Alberti et al. (1967) using 10 M H$_3$PO$_4$ and reflux times of 50 h. Propylamine intercalation compound, α-Ti(HPO$_4$)$_2$·2C$_3$H$_7$NH$_2$·H$_2$O (α-TiPPr), was obtained by placing α-TiP in an atmosphere saturated with propylamine vapor during 6 days at room temperature (Menéndez et al., 1990).

2.2. Sorption experiments

In bath, the α-TiP (or α-TiPPr) was equilibrated with europium nitrate solutions (T = 25.0 ± 0.1 °C, t = 72 h, solu-

tion/solid ratio = 20 mL/1 g). The prepared samples were designated as **TiP_x** (or **TiPPr_x**), where **x** indicates the molar concentration europium nitrate solution in the starting solutions, [Eu^{3+}]$_i$.

2.3. Characterization procedures

In residual solutions, the phosphorous and titanium contents were determined with a SpectraSpectrometer DCP-AEC. The powder X-ray diffraction (PXRD) patterns were recorded on Xpert Panalytical diffractometer with Cu Kα radiation (λ = 1.5418 Å). The samples were gently ground in an agate mortar in order to minimize the preferred orientation. A Mettler-Toledo thermogravimetric (TG) equipment (TGA/SDTA851^e) was used for the thermal analyses in oxygen dynamic atmosphere (50 mL/min) at a heating rate of 10 °C/min. In TG test, a Pfeiffer Vacuum ThermoStar™ GSD301T mass spectrometer was used to determine the evacuated vapors. Micrographs and X-ray microanalysis (SEM/EDX) were recorded with a JEOL JSM-6100 electron microscope operating at 20 kV coupled with an INCA Energy-200 energy dispersive X-ray microanalysis system (EDX) with Oxford PentaFET ultrathin window detector. The TEM studies were performed on a JEOL JEM-2100F field emission transmission electron microscope operated at an accelerating voltage of 200 kV and equipped with an ultra-high resolution pole-piece that provided a point-resolution better than 0.19 nm. Fine powder of the sample was dispersed in ethanol, sonicated and sprayed on a carbon coated copper grid, and then allowed to air-dry. Photoluminescence studies in air at RT were performed using a standard spectrofluorometer from Edinburgh Instruments model FLSP920, having a 450 W Xe lamp as the excitation source. The sample was placed between two quartz plates placed at 45° from the incident beam and the detector.

2.4. Structural modeling

The structural modeling of the material with the idealized formula [Eu(H$_2$O)$_6$]$_{2/3}$Ti(PO$_4$)$_2$·[(H$_2$O)$_6$]$_{1/3}$ has been performed according to the following steps. In the first stage, the bond lengths and angles of free H$_2$O and Eu(H$_2$O)$_6^{3+}$ species were optimized by DFT methods (GGA approximation and BLYP functional) by using the DMOL3 module implemented in BIOVIA Materials Studio (B.M.S., 2015). The results of the optimization are shown in Fig. S1. In the second step, the interlayer distance between the sheets of the starting structure α-Ti(HPO$_4$)$_2$·H$_2$O was expanded up to 12.0 Å (according to PXRD data) and then water molecules and hydrogenous atoms of HPO$_4$ groups were removed. Later, H$_2$O molecules and Eu(H$_2$O)$_6^{3+}$ cations were placed between the sheets, and subsequently, the supercell 1 × 3 × 1 of the expanded structure was built in order to keep fixed the idealized composition [Eu(H$_2$O)$_6$]$_{2/3}$Ti(PO$_4$)$_2$·[(H$_2$O)$_6$]$_{1/3}$. The position optimization of H$_2$O molecules, Eu(H$_2$O)$_6^{3+}$ cations and the sheets as rigid bodies were performed by means of molecular mechanics methods with the Forcite module (Universal force field) implemented in Biovia Materials Studio (B.M.S., 2015). In the final stage, the optimization was performed, leaving all atoms free for structure relaxation, by DFT methods (GGA approximation, PBE functional) using CASTEP module.

3. Results and discussion

PXRD analysis shows the both **TiP_10^{-4}** and **TiP_0.1** samples are highly crystalline and their patterns are identical, as seen in Fig. 1, with the first characteristic peak at $2\theta = 11.65°$ ($d_{002} = 7.58$ Å) corresponding to the interlayer distance of
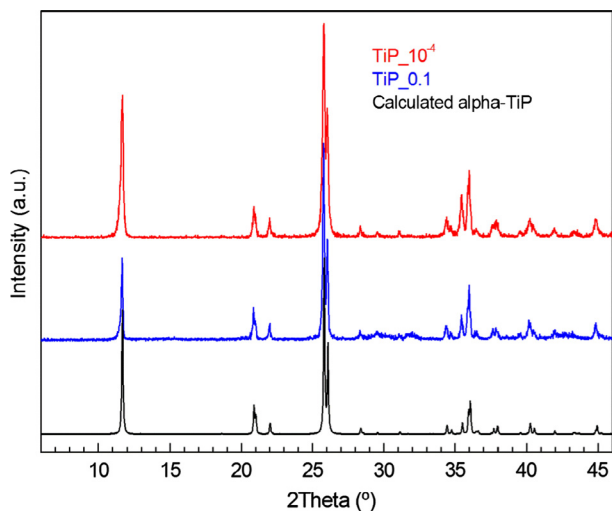
Figure 1 PXRD patterns of the samples **TiP_10^{-4}** (red) and **TiP_0.1** (blue), and calculated for α-TiP (black).

α-TiP. TEM images in Figs. 2a and b and 3a and b show that both samples maintain the typical platelet-like pseudo-hexagonal morphologies (length: 0.2–0.8 μm; thickness: 10–30 nm) similar to other metal phosphates (Manickam et al., 2004). However, in the case of **TiP_0.1**, an additional phase with nanorod-like morphology (thickness of *ca.* 10 nm) has been formed (for instance Fig. 3b and c). This phase was undetectable by PXRD as a consequence of its low content, poor crystallinity and nano crystallite size. In addition, the selected area electron diffraction (SAED) pattern of these nanorods found in **TiP_0.1** (Fig. 3d) has been indexed as standard hexagonal $EuPO_4$ H_2O phase (P3$_1$2$_1$, $a = 6.91$ Å, $b = 6.34$ Å; ICSD PDF4: 20-1044). In contrast, the only identified phase in the case of **TiP_10^{-4}** was α-TiP, as confirmed by SAED patterns in Fig. 2c and d. Furthermore, the chemical composition of $EuPO_4$ nanorods was confirmed by EDX analysis, revealing that both α-TiP and $EuPO_4$ phases are clearly distinguishable by EDX elemental mapping (see Fig. 4) in the case of **TiP_0.1**, while the only detectable element in the case of **TiP_10^{-4}** was Ti, P and O as seen in Fig. S2. In order to investigate the photoluminescence properties of **TiP_10^{-4}** and **TiP_0.1**, the emission spectra were obtained with $\lambda_{ex} = 394$ nm as shown in Fig. 5. The emission spectrum of **TiP_10^{-4}** does not show any transition line due to the sorption of Eu^{3+}. In contrast, the **TiP_0.1** spectrum shows the typical emission transitions of Eu^{3+}, which are attributed to $^5D_0 \rightarrow {}^7F_J$ (J = 0–4) transitions at, i.e. 580 nm ($^5D_0 \rightarrow {}^7F_0$), 592 nm ($^5D_0 \rightarrow {}^7F_1$), 616 nm ($^5D_0 \rightarrow {}^7F_2$), 650 nm
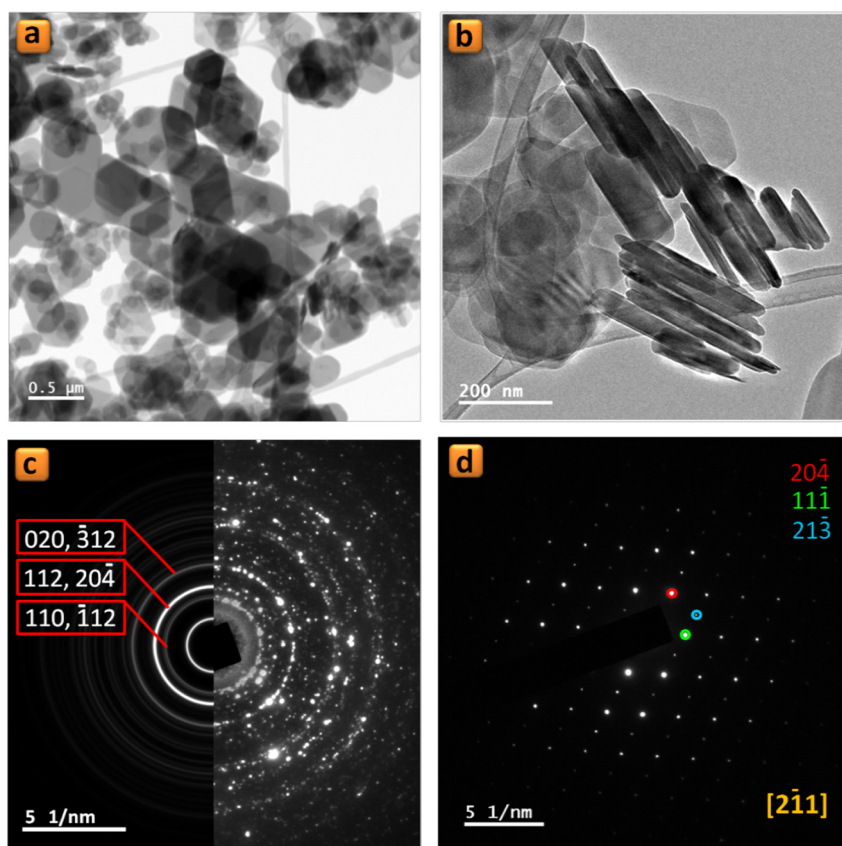
Figure 2 (a and b) TEM images, (c) selected area electron diffraction (SAED) patterns (left: simulated, right: experimental), and (d) nanobeam electron diffraction (NBD) pattern along [2–11] zone axis for a single particle of **TiP_10^{-4}** sample.

($^5D_0 \rightarrow {}^7F_3$), and 689 and 697 nm ($^5D_0 \rightarrow {}^7F_4$), with the most intense peak corresponding to the $^5D_0 \rightarrow {}^7F_2$ transition. These transition lines correspond basically to the $EuPO_4 \cdot H_2O$ nanorod phase. The observed low-intensity $^5D_0 \rightarrow {}^7F_0$ line is expected for Eu^{3+} in a site with C_n, C_{nv} and C_s symmetry. The high relative intensity of the hypersensitive $^5D_0 \rightarrow {}^7F_2$ transition is in accord with the Eu^{3+} local site symmetry (C_s), which is determined based on the crystal structure of hexagonal $EuPO_4 \cdot H_2O$ phase. Moreover, the $^5D_0 \rightarrow {}^7F_4$ transition is less intense than the $^5D_0 \rightarrow {}^7F_2$ transition but much more intense than the $^5D_0 \rightarrow {}^7F_1$ transition, and the same remarks have been made with Eu^{3+} in an asymmetric site with C_s symmetry in the case of $LaBO_3:Eu^{3+}$ with an orthorhombic aragonite structure (Binnemans, 2015).

From all the above data, we can conclude that the Eu^{3+} sorption process takes place only on the surface of α-TiP rather than in its interlayer space, because of the following summarized observations: (i) at high $[Eu^{3+}]_i$ no change in the interlayer distance of α-TiP has been observed by PXRD, and (ii) Eu^{3+} was undetectable by EDX analysis or by PL emission spectra at low $[Eu^{3+}]_i$.

In this context, α-TiP intercalated with propylamine (**TiPPr**) was selected as a potential material for efficient europium(III) uptake into layered tetravalent metal phosphates. For this purpose, **TiPPr** was treated with europium nitrate solutions at different concentrations until the equilibrium is reached. PXRD patterns of **TiPPr_10^{-4}** to **TiPPr_0.1**

(Fig. 6) show a structural order in the direction perpendicular to the plane of the sheet. In the range 0.0001–0.0625 M, the interlayer distance of the sheets remains substantially constant (16.0 Å), which is slightly lower than that of the starting material (16.9 Å, α-TiPPr) (Menéndez et al., 1990) as a consequence of a partial evacuation of the amine occupying the interlayered space. However, a new diffraction peak at $2\theta = 7.3°$ corresponding to d-spacing of 12.0 Å appears when the concentration is increased to 0.0750 M, which became the only observed peak when the $[Eu^{3+}]_i$ is raised to 0.1000 M. Moreover, the carbon content of the resulting solids (Table 1) continuously decreases with increasing concentration of europium nitrate in the starting solutions, in agreement with the results of STEM-EDS elemental mapping (Fig. S3), which obviously indicates the removal of the amine increases as the ionic strength of the solution increases. As a result, the behavior **TiPPr_x** can be divided into four different zones (red-blue-green-black), as illustrated in Table 1 and Fig. 6, depending on the concentration of Eu^{3+} in the initial solutions.

In the zone of low concentrations (red zone), the material consists of slightly wrinkled thin films (Figs. 7a–c and 8a–c) with lateral dimensions varying from about 0.1 μm to 1 μm and thicknesses of *ca.* 6.0 nm measured by atomic force microscopy. These thin films maintain a long-range order in the direction of the crystallographic *c*-axis as revealed by PXRD studies (Fig. 6), while a certain order is still maintained in *ab* plane as illustrated by the SAED pattern (see inset in
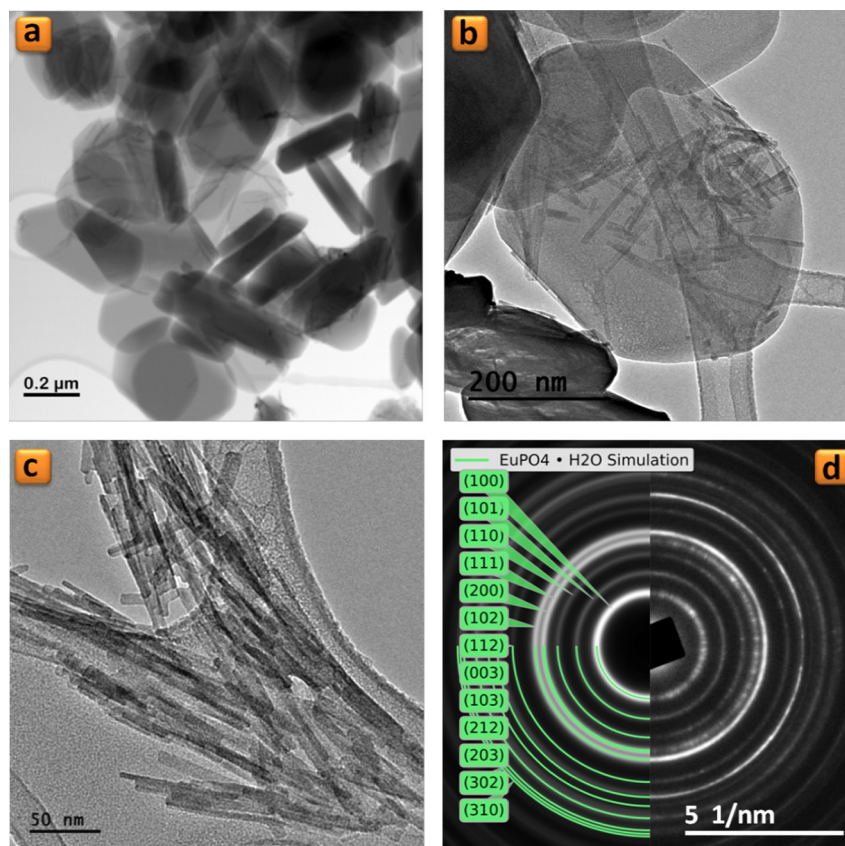

Figure 3 (a–c) TEM images of **TiP_0.1** sample and (d) selected area electron diffraction (SAED) patterns (left: simulated, right: experimental) corresponding to the image (c).
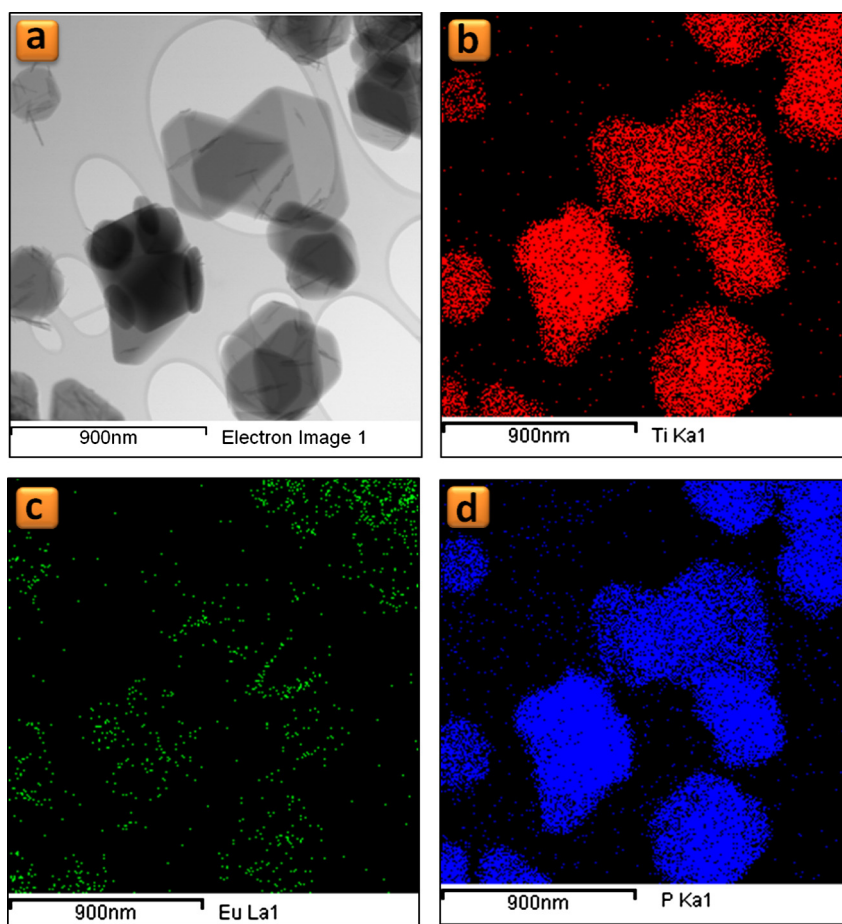
Figure 4 Elemental mapping for **TiP_0.1** sample: (a) Bright field-STEM images, (b) Ti-Kα_1 map, (c) Eu-Lα_1 map and (d) P-Kα_1 map.
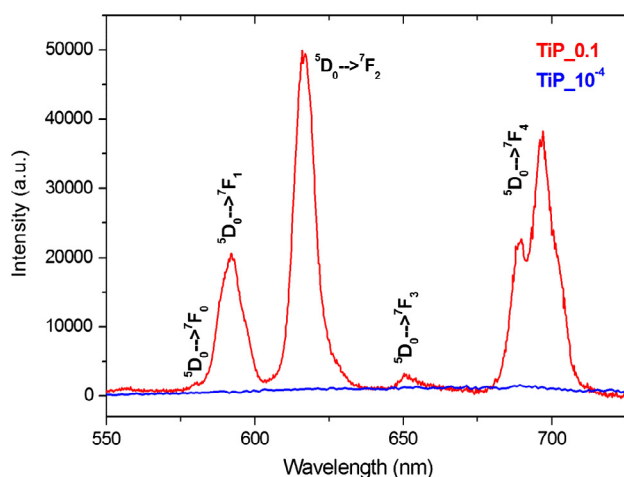
Figure 5 Emission spectra of the samples **TiP_0.1** (red) and **TiP_10^{-4}** (blue) obtained up excitation at 394 nm.
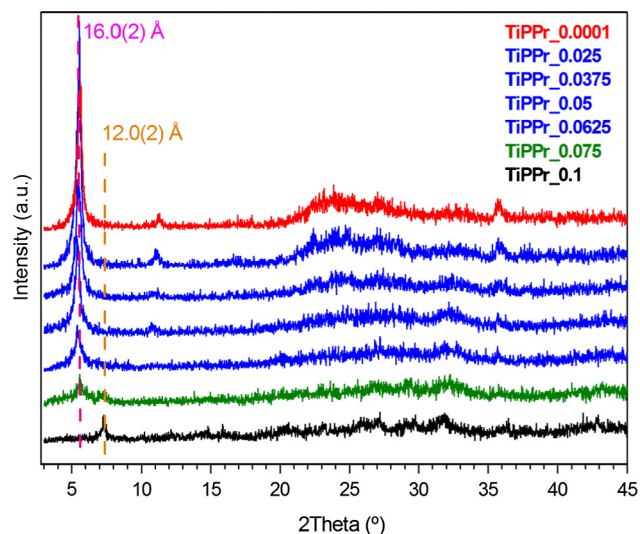
**Figure 6** PXRD patterns of the **TiPPr_x** samples.

Fig. 8a–c). Moreover, the propylamine content decreases in this red zone (see Table 1 and Fig. 6) compared to the starting material **TiPPr** with interlayer distance 16.9 Å (Menéndez et al., 1990). However, the presence of Eu^{3+} in these films was undetectable by STEM-EDS elemental mapping as shown in Fig. 9a and b, in agreement with the emission spectrum (for

instance **TiPPr_10^{-4}** spectrum in Fig. 10) which does not show any transition line due to the sorption and/or intercalation of Eu^{3+}.

In the region of intermediate concentrations (blue zone), the layers are stacked in the direction perpendicular to the

Table 1 Experimental data for samples obtained when α-TiPPr was equilibrated with europium(III) nitrate solutions of several concentrations ($[Eu^{3+}]_i$): Carbon content (C), total weight loss at 1000 °C in air atmosphere (Δm) obtained by TG-analysis, and phosphorus (P) and titanium (Ti) contents in a non-centrifugal fraction expressed as concentration (mg/L) and percentage (%) of the total content in the starting material.

| Sample	$[Eu^{3+}]_i$ (mol/L)	C (%)	Δm (%)	P (mg/L)	Ti (mg/L)	P (%)	Ti (%)
TiPPr_10^{-4}	0.0001	13.4	33.8	6254	4374	76	69
TiPPr_10^{-3}	0.001	13.4	37.4	5489	3903	67	61
TiPPr_10^{-2}	0.01	12.7	34.7	4595	3119	56	49
TiPPr_0.025	0.025	11.9	36.1	1401	734	17	11
TiPPr_0.0375	0.0375	9.9	32.7	761	273	9	4
TiPPr_0.05	0.05	8.3	29.8	409	< 1	5	< 1
TiPPr_0.0625	0.0625	5.8	26.6	177	< 1	2	< 1
TiPPr_0.075	0.075	4.9	25.7	82	< 1	1	< 1
TiPPr_0.1	0.1	2.5	25.0	24	< 1	< 1	< 1
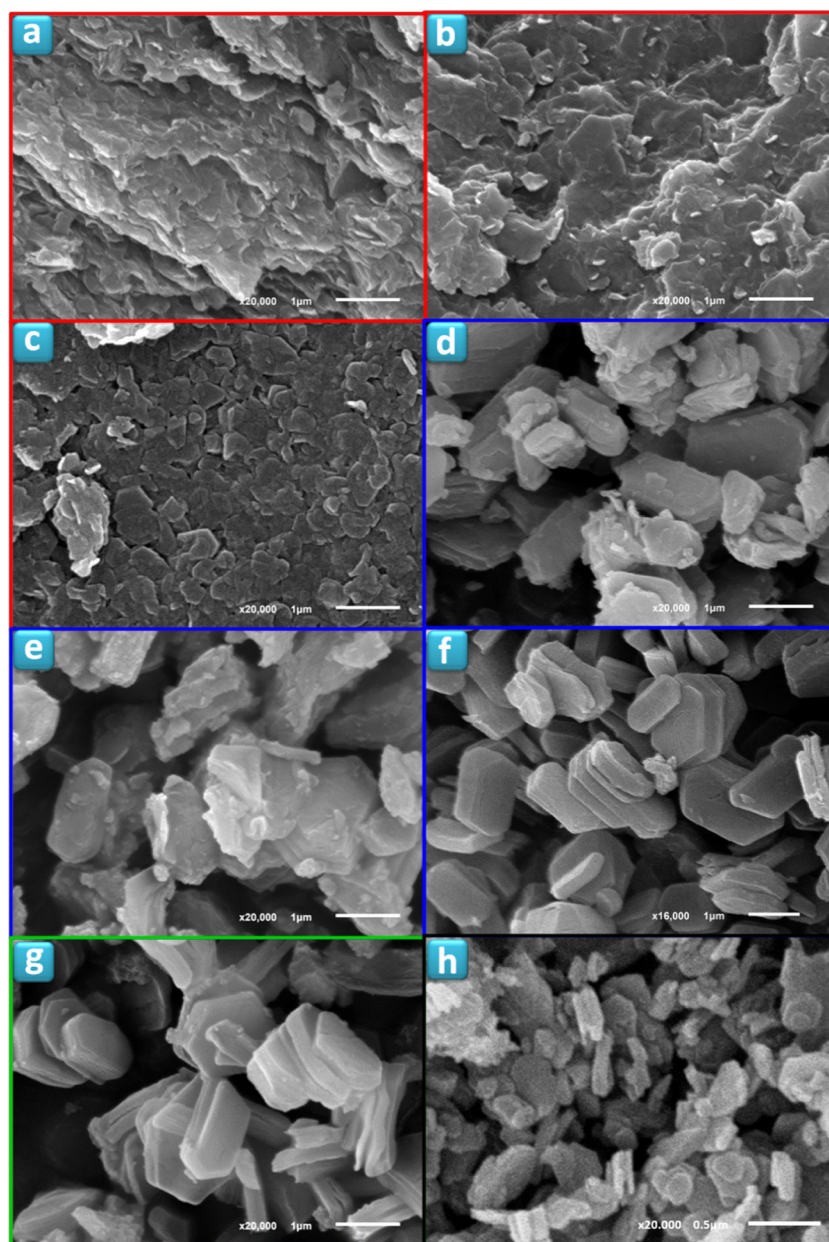
Figure 7   SEM images of **TiPPr_x** samples ($x = 10^{-4}$ (a), 10^{-3} (b), 0.01 (c), 0.025 (d), 0.0375 (e), 0.0625 (f), 0.075 (g) and 0.1 (h)).
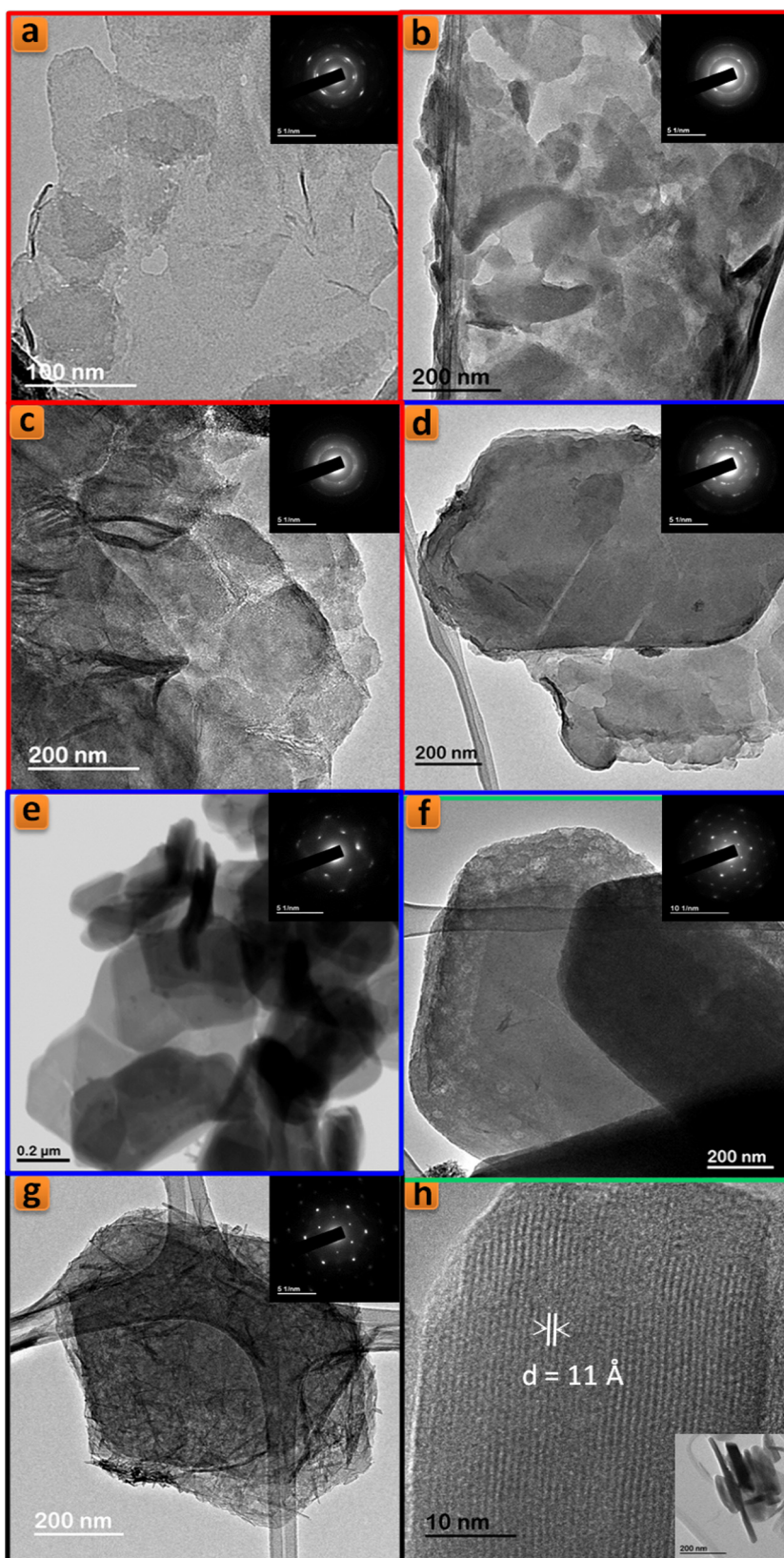
Figure 8   TEM images of **TiPPr_x** samples ($x = 10^{-4}$ (a), 10^{-3} (b), 0.01 (c), 0.025 (d), 0.05 (e), 0.075 (f) and 0.1 (g and h)).

plane of the titanium phosphate sheet, where the interlayer distance is slightly lower than in the starting material **TiPPr**, but it is essentially constant (16.0 Å) as shown in Fig. 6, while the

pseudo-hexagonal morphologies are preserved (Figs. 7d–f and 8d and e). The amine content gradually decreases (reflected in the decrease in carbon content, see Table 1); thus,
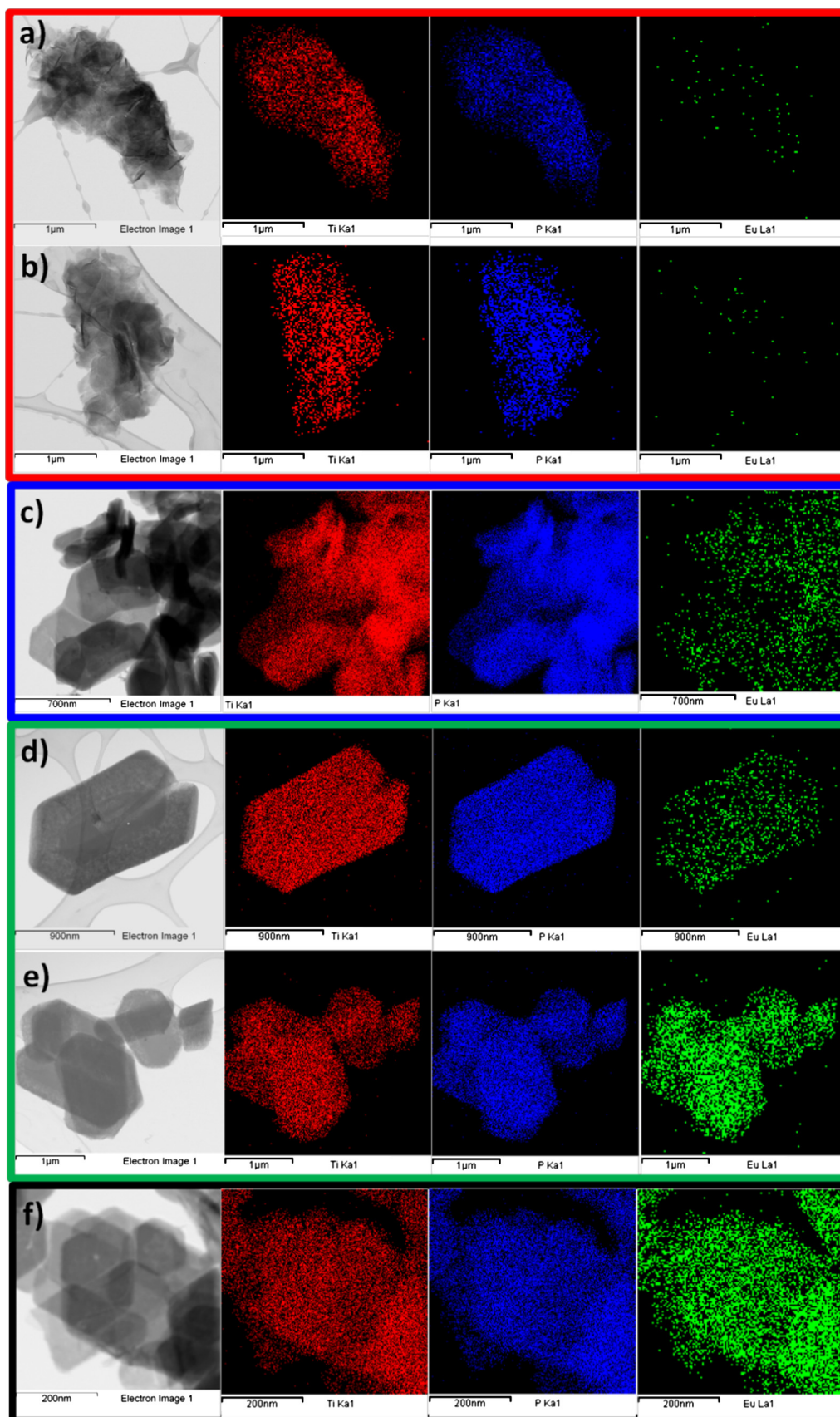
Figure 9   STEM-EDS elemental mapping of **TiPPr_x** samples ($x = 10^{-4}$ (a), 10^{-3} (b), 0.05 (c), 0.075 (d and e) and 0.1 (f)); Ti-Kα_1 (red), P-Kα_1 (blue) and Eu-Lα_1 (green) elemental maps.

the Eu-content increases in the solid phase as confirmed by EDX mapping (Fig. 9c) and by the presence of $^5D_0 \rightarrow {^7F_J}$ ($J = 0$–4) transition peaks in the emission spectrum of **TiPPr_0.05** (Fig. 10). Assuming that an ion-exchange process is taking place between the propylammonium cations, $C_3H_7NH_3^+$, and the hexahydrate species of europium, $[Eu(H_2O)_6]^{3+}$, the following tentative formula, $(C_3H_7NH_3)_{2-3y}[Eu(H_2O)_6]_y Ti(PO_4)_2 \cdot [(H_2O)_6]_{y/2}$, has been proposed for the resulting materials. This process proceeds *via* the formation of solid solutions, where $C_3H_7NH_3^+$ species act as pillars adopting a bilayer structure with the tilt angle of the alkyl chain of *ca.* 50° relative to the plane of the titanium phosphate sheet, and occupying a fraction of the pseudo-zeolitic cavities of the titanium phosphate, while the rest of the cavities would be occupied by $[Eu(H_2O)_6]^{3+}$ species. The calculated total mass loss decreases from 36.65% ($y = 0.15$) to 26.69% ($y = 0.55$), in a good agreement with experimental data: 36.1–26.6% obtained from TGA data (see Table 1).

At higher concentration (zones shown in green and black), the particles maintain their pseudo-hexagonal morphologies (Fig. 7g and h and 8f and g), and besides the presence of an interlayer distance of 16.0 Å in the case of **TiPPr_0.075**, the appearance of a new phase with *d*-spacing of 12.0 Å is also observed (Fig. 6), which is the only one that remains in the black zone (**TiPPr_0.1**). HRTEM (Fig. 8h) shows a *d*-spacing of *ca.* 11.0 Å, close to the value obtained by PXRD, and this difference is due to the instantaneous dehydration followed by a fast amorphization of the particles under the electron beam irradiation. In this latter zone, the low carbon content suggests that almost all the alkylammonium cations have been involved in the ion-exchange process, thus leading to the formation of a material with the idealized formula $[Eu(H_2O)_6]_{2/3}Ti(PO_4)_2 \cdot [(H_2O)_6]_{1/3}$, where $[Eu(H_2O)_6]^{3+}$ occupying 2/3 of the pseudo-zeolitic cavities so as to counteract the negatively charged titanium phosphate layer. The rest of the pseudo-zeolitic cavities (1/3 of the total) will be occupied by water molecules. Based on this expected formula, the calculated mass loss of 24.15% is in good accordance with the experimental mass loss of 25.0%. Moreover, STEM-EDS elemental mapping of **TiPPr_0.075** (Fig. 9d and e) and **TiPPr_0.1** (Fig. 9f), corresponding to the green and black zones, respectively, shows a significant increase in Eu-content compared to the blue zone, and it is noteworthy that in the case of green zone there are particles with low and high Eu-content (Fig. 9d and e), which could be related to the presence of two phases with different basal spacing (16.0 Å and 12.0 Å), as revealed by PXRD analysis (Fig. 6). On the other hand, the emission spectrum of **TiPPr_0.1** (Fig. 10) still shows the expected $^5D_0 \rightarrow {^7F_J}$ ($J = 0$–4) transition peaks but with a decrease in their relative intensities compared to the spectrum of the blue zone, which is probably associated with the absence of propylamine and high degree of hydration leading to emission quenching. The emission spectra of samples **TiPPr_0.05** and **TiPPr_0.1** show the five possible luminescence bands expected in the registered spectral region. The number of lines observed for the $^5D_0 \rightarrow {^7F_J}$ ($J = 0$–4) transitions in the luminescence spectrum allows determining the site symmetry of the Eu^{3+} ion (Binnemans, 2015). The highest energy $^5D_0 \rightarrow {^7F_0}$ line is very weak, in agreement with Judd–Ofelt theory (the transition should only be expected to be observed for Eu^{3+} in a site with C_n, C_{nv} or C_s symmetry). The very intense hypersensitive transition $^5D_0 \rightarrow {^7F_2}$ indicates that the Eu^{3+} is not at a site with a center of symmetry. In addition, the transition $^5D_0 \rightarrow {^7F_3}$ has very weak intensity since they are forbidden by the selection rule of ΔJ for electric dipole transitions.

The colloidal suspensions (non-centrifugal phases) of **TiPPr_10^{-4}** to **TiPPr_0.1** have been analyzed by ICP-MS. The results (Table 1) show that the concentrations of both P and Ti decrease with increasing $[Eu^{3+}]_i$. In the red zone (low concentrations), about three quarters of the starting material **TiPPr** are found in the liquid phase, mainly in the form of nanometric colloidal TiP monolayers, although a portion of this ¾ is dissolved due to the partial hydrolysis of the starting material. While in the blue zone (intermediate concentrations), the amount of the nanometric colloidal TiP suspension decreases drastically with increasing $[Eu^{3+}]_i$, which is reflected in the decrease in P and Ti content in the liquid phase. The fact that the percentage of P in solution is higher than Ti, in both the red and blue zones, indicates the existence of hydrolysis processes of the titanium phosphate, which may give rise to
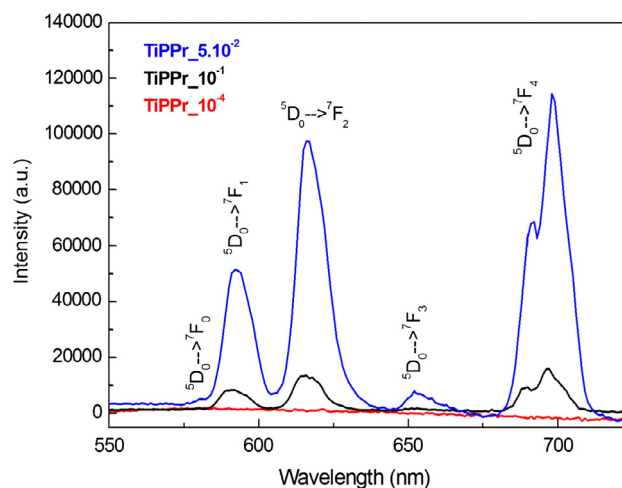
Figure 10 Emission spectra of **TiPPr_10^{-4}** (red), **TiPPr_0.05** (blue) and **TiPPr_0.1** (black), obtained up excitation at 394 nm.
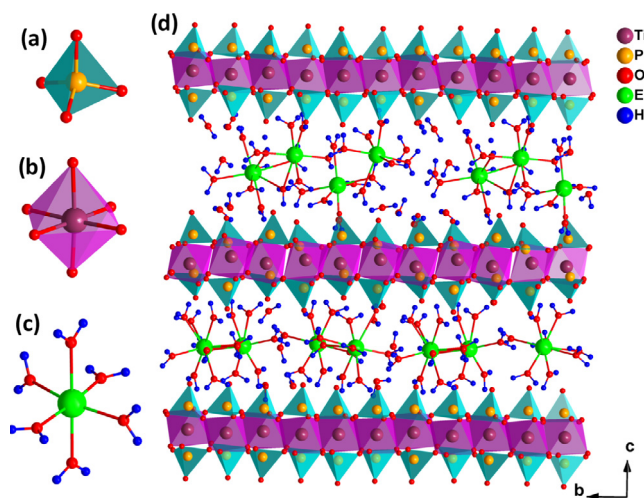
Figure 11 Perspective view of the coordination environment of P (a), Ti (b), Eu (c) and the projection of the structural model of $[Eu(H_2O)_6]_{2/3}Ti(PO_4)_2 \cdot [(H_2O)_6]_{1/3}$ along the *a*-axis (d).

the formation of aqueous phosphate species and precipitation of titanium dioxide gels. Finally, in the green zone, and especially in the black one, high $[Eu^{3+}]_i$ causes the liquid phase to be substantially free of P and Ti. However, in the solid phase, and beside the hypothetical ion-exchange phase $[Eu(H_2O)_6]_{2/3}Ti(PO_4)_2 \cdot [(H_2O)_6]_{1/3}$, it shall be present variable amounts of $EuPO_4 \cdot H_2O$ (for instance, see nanorods in Fig. 8g) and $TiO_2 \cdot nH_2O$ (not observed by TEM), coexisting with a residual phase containing propylamine (Fig. S3d).

The final structural model proposed by using DFT calculations for the material with the idealized formula $[Eu(H_2O)_6]_{2/3}Ti(PO_4)_2 \cdot [(H_2O)_6]_{1/3}$ is shown in Fig. 11. Its structure consists of PO_4 tetrahedral (Fig. 11a) and TiO_6 octahedral (Fig. 11b) units connected through their vertices, giving rise to 2D-dimensional inorganic sheets, which are still closely related to those of the α-TiP. The hexahydrate species of europium, $[Eu(H_2O)_6]^{3+}$ (Fig. 11c), and non-coordinated H_2O molecules occupy the interlamellar space, with the average Eu–O bond distance and Eu–Eu distance between adjacent $[Eu(H_2O)_6]^{3+}$ cations of 2.58 Å and 4.91 Å, respectively.

4. Conclusions

In summary, we have shown that when α-TiP is used as sorbent the Eu^{3+} uptake process is limited to its surface, being the interlayer space inaccessible to the hexahydrate $[Eu(H_2O)_6]^{3+}$ cations. However, the Eu^{3+} uptake is considerably improved with α-TiPPr as a consequence of an ion-exchange process into the expanded interlayer space, involving $C_3H_7NH_3^+$ cations and $[Eu(H_2O)_6]^{3+}$ species, with the formation of α-$[Eu(H_2O)_6]_{2/3}Ti(PO_4)_2 \cdot [(H_2O)_6]_{1/3}$ as final product.

Acknowledgments

Appendix A. Supplementary material

Supplementary data associated with this article can be found, in the online version, at http://dx.doi.org/10.1016/j.arabjc.2016.07.013.

References

Alberti, G., Cardini-Galli, P., Costantino, U., Torracca, E., 1967. Crystalline insoluble salts of polybasic metals. 1. Ion-exchange properties of crystalline titanium phosphate. J. Inorg. Nucl. Chem. 29, 571.

Alfonso, B.F., Trobajo, C., Salvadó, M.A., Pertierra, P., García-Granda, S., Rodríguez-Fernández, J., Blanco, J.A., García, J.R., 2005. Synthesis and characterization of α-titanium phosphate/propylamine intercalation compounds containing transition-metal ions. Z. Anorg. Allg. Chem. 631, 2174.

Álvarez, C., Llavona, R., García, J.R., Suárez, M., Rodríguez, J., 1987. Lamellar inorganic ion-exchangers. Proton-copper(II) ion-exchange in γ-titanium bis(hydrogenphosphate). J. Chem. Soc., Dalton Trans., 2045

B.M.S., 2015. <http://accelrys.com/products/collaborative-science/biovia-materials-studio/>.

Binnemans, K., 2015. Interpretation of europium(III) spectra. Coord. Chem. Rev. 295, 1.

Clearfield, A., Díaz, A., 2015. Zirconium phosphate nanoparticles and their extraordinary properties. In: Brunet, E., Colón, J.L., Clearfield, A. (Eds.), Tailored Organic–Inorganic Materials. John Wiley & Sons Inc, Hoboken, New Jersey.

Espina, A., García, J.R., Guil, J.M., Jáimez, E., Parra, J.B., Rodríguez, J., 1998a. Calorimetric study of amine adsorption on α- and γ-titanium phosphate. J. Phys. Chem. B 102, 1713.

Espina, A., Jáimez, E., Khainakov, S.A., Trobajo, C., García, J.R., Rodríguez, J., 1998b. Synthesis of new n-alkylamines intercalation compounds with α-titanium phosphate. Process selectivity and structural and morphological characterization. Chem. Mater. 10, 2490.

García-Granda, S., Khainakov, S.A., Espina, A., García, J.R., Castro, G.R., Rocha, J., Mafra, L., 2010. Revisiting the thermal decomposition of layered γ-titanium phosphate and structural elucidation of its intermediate phases. Inorg. Chem. 49, 2630.

Llavona, R., Suárez, M., García, J.R., Rodríguez, J., 1989. Lamellar inorganic ion-exchangers. Alkali-metal ion exchange on α- and γ-titanium phosphate. Inorg. Chem. 28, 2863.

Mafra, L., Paz, F.A.A., Rocha, J., Espina, A., Khainakov, A., García, J.R., Fernández, C., 2005. Structural characterization of layered γ-titanium phosphate $(C_6H_{13}NH_3)[Ti(HPO_4)(PO_4)] \cdot H_2O$. Chem. Mater. 17, 6287.

Mafra, L., Rocha, J., Fernández, C., Castro, G.R., García-Granda, S., Espina, A., Khainakov, S.A., García, J.R., 2008. Characterization of layered γ-titanium phosphate $(C_2H_5NH_3)[Ti(H_{1.5}PO_4)(PO_4)]_2 \cdot H_2O$ intercalate: a combined NMR, synchrotron XRD, and DFT calculations study. Chem. Mater. 20, 3944.

Manickam, M., Minato, K., Takata, M., 2004. Synthesis and electrochemical properties of $TiNb(PO_4)_3$ cathode materials for lithium secondary batteries. J. Electroanal. Chem. 562, 1.

Menéndez, A., Bárcena, M., Jáimez, E., García, J.R., Rodríguez, J., 1993. Intercalation of n-alkylamines by γ-titanium phosphate. Synthesis of new materials by thermal treatment of the intercalation compounds. Chem. Mater. 8, 1078.

Menéndez, F., Espina, A., Trobajo, C., Rodríguez, J., 1990. Intercalation of n-alkylamines by lamellar materials of the α-zirconium phosphate type. Mater. Res. Bull. 25, 1531.

Mrad, O., Abdul-Hadi, A., Arsan, H., 2011. Preparation and characterization of three different phases of zirconium phosphate: study of sorption of ^{234}Th, ^{238}U, ^{134}Cs. J. Radioanal. Nucl. Chem. 287, 177.

Ortiz-Oliveros, H.B., Flores-Espinosa, R.M., Ordóñez-Regil, E., Fernández-Valverde, S.M., 2014. Synthesis of α-$Ti(HPO_4)_2 \cdot H_2O$ and sorption of Eu (III). Chem. Eng. J. 236, 398.

Salvadó, M.A., Pertierra, P., García-Granda, S., García, J.R., Rodríguez, J., Fernández-Díaz, M.T., 1996. Neutron powder diffraction study of α-$Ti(HPO_4)_2 \cdot H_2O$ and [alpha]-$Hf(HPO_4)_2 \cdot H_2O$; H-atom positions. Erratum. Acta Cryst. B52, 896.

Trobajo, C., Suárez, M., Rodríguez, J., 1991. Quantitative extraction of uranium(VI) in aqueous solutions with n-alkylamine intercalates of γ-titanium phosphate. J. Radioanal. Nucl. Chem. 149, 67.

Zhuravlev, I., Zakutevsky, O., Psareva, T., Kanibolotsky, V., Strelko, V., Taffet, M., Gallios, G., 2002. Uranium sorption on amorphous titanium and zirconium phosphates modified by Al^{3+} or Fe^{3+} ions. J. Radioanal. Nucl. Chem. 254, 85.